Journal of Solid State Electrochemistry (2024) 28:3713–3730
https://doi.org/10.1007/s10008-024-05955-x

ORIGINAL PAPER

The fabrication of hemoglobin encapsulation into ZIF-67 and its electrochemical property

Jian Ming Wang[1] · Xue Qing Chu[1] · Han Zeng[1]

Received: 1 March 2024 / Revised: 1 June 2024 / Accepted: 2 June 2024 / Published online: 15 June 2024

Abstract

Hemoglobin (Hb)-based electrodes were fabricated using a Co-based complex with cobalt nitrate hexahydrate and 2-methylimidazole as fundamental elements to accommodate enzymes via the conventional solvothermal method. The binding of redox protein molecules to metal–organic framework-based complexes occurred through a synergistic effect of hydrogen bonding and competitive complexation, resulting in a partially oriented arrangement of metalloprotein molecules with enhanced hydrophilicity. The Hb–Co complex was formed via a typical electrostatic quenching mode with a moderate binding capacity. The native heme site within Hb and the cofactor of the enzyme ligated with ZIF-67 were involved in the electron shuttle process. The former electro-active site displayed favorable electrochemical activity (apparent heterogeneous electron transport rate: 0.1 s^{-1}). The inherent configuration of the cofactor in the protein and abnormal electrocatalytic activity of the incorporated protein were considerably maintained. The electrocatalytic efficiency could be affected by both the protein and the Co-based complex. The key step in restraining the electrochemical sensing performance was the H_2O_2 mass transfer procedure.

Keywords Metal–organic framework material · Hemoglobin · Competitive complexation · Electrocatalysis · H_2O_2 sensing efficiency

Introduction

Electrochemical sensors are widely used in various fields, including biomedical monitoring and pollutant measurement/control, owing to their simplicity, rapid responses, and high sensitivity. The roles of the functional groups within the sensors (e.g., biosensing elements and electron transportation sites) and the mutual interactions between the functional groups are particularly important for extending the application scope and improving the practical value of electrochemical sensors [1–3]. Biomacromolecules, such as redox proteins, are regarded as suitable candidates to act as biosensing sites within electrochemical sensors [4–9]. Heme proteins are representative redox enzymes that act as bioelectrocatalysts and core sensing elements in electrochemical sensors. Hemoglobin (Hb), a member of the heme protein family, can carry and bind O_2 molecules. Its relatively simple structure and low cost have contributed to its wide exploration and extensive probing. Hb has the same active site (i.e., Fe–porphyrin complex as the heme site) and a backbone distribution similar to those of other isozyme molecules, such as horseradish peroxidase and myoglobin, facilitating elucidation of the physiological activity of the heme protein family. However, the interactions (i.e., H-bond interactions, competitive ligation, and covalent coupling) between the biomacromolecules, and their supporters have considerable effects on the physicochemical idiosyncrasies and sensing efficacies of the as-prepared biomacromolecule-based electrodes. To the

Highlights
- The combination of hemoglobin with ZIF-67 should be classified into a typical static fluorescence quenching mode with the moderate binding intensity.
- The competitive ligation of heme protein with ZIF-67 could form the partially orientated protein array onto ZIF-67 with improved hydrophilicity from the unique electron distribution of Co element.
- The mutual interactions between hemoglobin and ZIF-67 would not impose seriously negative effect on the electro-catalytic efficiency and the favorable sensing performance to hydrogen peroxide could be kept to great extent.

✉ Han Zeng
zenghan1289@163.com

[1] Xinjiang Key Laboratory of Energy Storage and Photoelectrocatalytic Materials, Chemistry and Chemical Engineering Academy, Xinjiang Normal University, Urumuqi 830054, Xinjiang Uyghur Autonomous Region, People's Republic of China

best of our knowledge, relevant research remains scarce [10–12].

Metal–organic framework (MOF) materials are commonly used matrices to accommodate biomacromolecules (e.g., redox proteins) because of their unique traits such as moderate porosity, high specific surface area, and facile processing. Zeolite imidazole framework (ZIF) materials are typical MOF materials with tetrahedral frameworks resulting from the cross-linking of transition metal atoms with imidazolate groups as ligands. A ZIF with a novel function was previously prepared via simple modification of the cross-linking procedure used to form a MOF material [13]. This ZIF material demonstrated higher chemical stability and a more sophisticated structure than other MOF materials. However, the inferior conductivity of MOFs limits their application in the design and preparation of electrochemical sensors. The H-bond interaction between the surface hydrophilic groups on the biomolecule and ZIF as well as the competitive ligations of metal elements within ZIF/redox protein molecules with the surrounding ligands are crucial factors in determining the efficacy of the electrochemical sensors prepared, as described. A better understanding of the impacts of such interactions on the redox proteins involved in electrocatalytic dynamics is essential [14–18].

Based on previous concepts, ideas, and analyses, the purpose of this study was to investigate the effects of competitive complexation between metal atoms and imidazolyl groups or surface amino acid residues as ligands on the dynamics of enzyme-induced electrocatalysis. ZIF-67, with a tetrahedral skeleton, was proposed to accommodate heme proteins by competitive ligation. A heme-protein-based electrode was prepared using traditional drop-casting methods. The protein aggregation state of ZIF-67, structural traits of ZIF-67 with protein immobilization, electrochemical behavior, and electrocatalytic efficiency of the protein-based redox electrode were investigated and evaluated using spectroscopy, microscopy, and electrochemistry. The primary objective of this study was to elucidate the influence of competitive ligation between the metal protein and ZIF-67 on the mechanism of charge transportation and substrate-binding transformation. The current study will contribute to advances in biomimetic electrochemical instruments and better comprehension of the essence of the physiological activities of bio-organisms.

Experiment

Reagents and apparatus

We purchased 2-methylimidazole (Hmim) from Aladdin Chemical Reagent Co., Ltd. (Shanghai, China). Analytical-grade cobalt nitrate hexahydrate was supplied by Titan Chemical Reagents Co., Ltd. (Shanghai, China). Hb from bovine blood (molecular mass: ~ 64,500 $g \cdot mol^{-1}$, aboriginal enzyme-induced activity to H_2O_2 reduction: 1.2 $U \cdot mg^{-1}$) and KBr with a purity of over 90% were purchased from Sigma-Aldrich Chemical Reagent Co., Ltd. (USA). Chitosan (CTS; with analytical purity, degree of deacetylation: ≥ 90% and molecular mass: ~ 250,000 $g \cdot mol^{-1}$) as film former was supplied by Sinopharm Chemical Reagent Co., Ltd. (China). The Clark O electrode was obtained from Hansatech (UK). High-purity N gas was supplied by Beijing Fen Gas Industrial Co., Ltd. (Beijing, China). The 2K15 type ultraspeed centrifuge was obtained from Sigma (St. Louis, MO, USA). The objective electrode used in this study was a glassy C electrode (GCE), 3 mm in diameter. An Ag/AgCl electrode in a saturated KCl aqueous solution was used as the reference electrode, and a Pt wire was utilized as the counter electrode. Both electrodes were supplied by Tian-Jin Aida Heng-Sheng Industrial and Commercial Co., Ltd. (China). The bare GCE was pretreated, and the active regions of the as-prepared electrodes were determined using a previously reported protocol [19]. The electrolyte used throughout the electrochemical tests and the electrocatalytic/photoelectrocatalytic experiments was 0.2 M phosphate buffer solution (PBS).

A Hitachi z2000 atomic absorption spectrometer equipped with a graphite furnace atomic absorption spectrophotometer (main frame: single-beam flame) was obtained from Hitachi (Japan). A SU8010 field emission scanning electron microscope (FE-SEM) operating at an accelerating voltage of 5.0 kV and a U-3310 ultraviolet–visible (UV–Vis) spectrophotometer with a cuvette thickness of 1.0 cm were provided by Hitachi (Japan). An SEM with an energy dispersive spectrometer was acquired from Oxford Instruments (UK). A D2PHASER diffractometer with a Cu-Kα radiation source (wavelength of 1.54 Å) and TENSOR27 Fourier transform infrared (FTIR) spectrometer (KBr panel) were provided by BRUKER (Germany). An X-ray spectrometer of Super-X class and an X-ray photoelectron spectrometer of ESCALAB Xi+ type were supplied by Thermo Fisher Co., Ltd. (USA). A Chirascan spectropolarimeter obtained from Applied Photophysics was used throughout the circular dichroism (CD) experiments. A 150 W Xe lamp and an air-cooling device were installed in the spectropolarimeter. The thickness of the quartz cuvette used in the experiments was 10.0 mm. A Cary Eclipse spectrofluorometer was purchased from Varian (USA). A Zahner Zennium electrochemical analyzer was provided by Kronach (Germany). A CHI-660E electrochemical workstation was purchased from Chen-Hua Co., Ltd. (Shanghai, China). An electrochemical platform with an AFMSRCE rotating glassy C disk electrode system was purchased from Pine Company (USA).

Preparation and characterization of ZIF-67 with Hb accommodation

The solvothermal method was employed to synthesize the MOF, with ZIF-67 as the enzyme carrier. The specific route for preparing the MOF has been described previously [20]. A general description of the synthetic procedure for ZIF-67 is as follows: 0.718 g of cobalt nitrate hexahydrate was dissolved in 50 mL of methanol, and the solution was mixed swiftly with the methanol solution with 1.62 g dissolved Hmim under vigorous agitation for 30 min. The reactant system was incubated at room temperature for 20 h. The precipitate was isolated from the feculent system by centrifugation at 8000 rpm. The secured sediment was washed with methanol several times, and it was dried in a vacuum drier at 60 °C for 10 h to obtain the target MOF material, ZIF-67. Purple ZIF-67 powder (120 mg) was added to 18 mL of neutral PBS, and the mixture was subjected to ultrasonic dispersion for 10 min to secure an evenly dispersed phase. Next, 4.0 mL PBS with a Hb concentration of 5.0 mg·mL^{-1} was poured into the discrete, and the mixture was stirred acutely for 10 min. The discrete mucous was stored overnight in a refrigerator to allow adequate interaction between the Hb molecules and the MOF to occur. The solid phase was washed twice with methanol and distilled water, and the ZIF-67 complex with Hb was recovered by centrifugation at 6000 rpm. The prepared fluid was designated as Hb@ZIF-67. Next, 10.0 µL of the Hb@ZIF-67 viscous fluid was pipetted onto the polished surface of the GCE. Then, 2.0 µL of CTS film-forming reagent was coated onto the electrode surface with a Hb@ZIF-67 cap composite. The supporting electrode, mantled by a composite of ZIF-67 with Hb attachment, was placed in an inverted beaker for air-drying under indigenous pressure and room temperature. The electrode prepared using Hb is referred to as Hb@ZIF-67/GCE. The ZIF-67/GCE reference electrode was prepared using a similar procedure, except that Hb was not introduced. The Hb@ZIF-67/GCE preparation procedure is shown in Fig. 1.

The enzyme accommodation capacity of the MOF ZIF-67 and the leakage of Hb from its matrix were determined using graphite furnace atomic absorption spectrometry (GFAAS). The parameters were determined by monitoring the change in the dissolved Fe-ion content in the stock solution before and after Hb attachment to ZIF-67. The wavelength sweeping range was modulated in the range of 190–900 nm. Descriptions of the specific operation and estimation of the enzyme immobilization weight can be found elsewhere [21, 22]. The morphological features of ZIF-67 with Hb entrapment and the dimensions of ZIF-67 alone were characterized using SEM. Characterization was performed using an FE-SEM equipped with a Pt stand. The instrument was operated at an accelerating voltage of 5.0 kV, with a secondary electron resolution of 1.0 nm at 15.0 kV. The SEM samples were prepared by

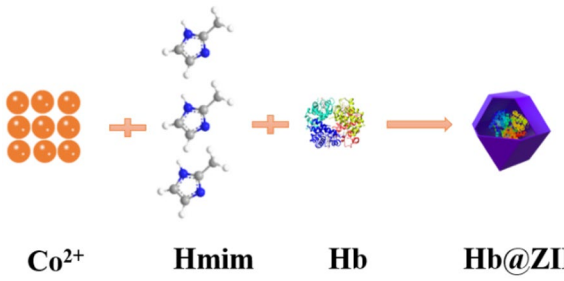

Fig. 1 Schematic illustration of the composition and preparation procedure for biocomposite (ZIF-67 with Hb) encapsulation

milling the as-prepared products (ZIF-67 and MOF material with Hb retention) into powder and adhering the sample powder onto the stand with a conductive adhesive. X-ray photoelectron spectroscopy (XPS) was utilized to analyze the nature of the surface chemical bonding between ZIF-67 and the adsorbed Hb. The peculiarities of the crystalline planes of the as-prepared samples were investigated by employing an X-ray diffractometer equipped with a Cu-Kα radiation source (wavelength: 1.54 Å, tube voltage: 30.0 kV, and tube current: 10.0 mA). The scope of the sweeping angle (2θ) was confined in the range of 5–50°. FTIR measurements were performed to characterize the structural features of the as-prepared samples, and the reagent was pressed into a KBr powder to produce sample tablets. The change in the configuration of redox sites within the heme protein and the specific activity of Hb-containing catalysts in H_2O_2 reduction were investigated and determined by UV–Vis spectroscopy. The operational procedures were performed according to experimental protocols described elsewhere [19]. Furthermore, the membrane rigidity of the MOF material with Hb fixation was evaluated by UV–Vis spectroscopy; the specific operation has been described previously [22]. CD was used to study the surface physicochemical characteristics of ZIF-67 with Hb attachment. The wavelength utilized in the CD tests was regulated within the range of 200–450 nm. To prepare a uniform and stable dispersed phase, 4 mg of the Hb@ZIF-67 nanocomplex was transferred to 4 mL of PBS at pH 7.0 and stirred magnetically for 30 min. The dispersion was stored overnight in a refrigerator at 0 °C to prepare the nanocomplex with Hb inclusion. We employed 300 mL of dispersion for each CD test. Fluorescence emission spectrometry (FRS) was performed to assess the effects of the interactions between immobilized Hb molecules and ZIF-67 on the structural parameters of Hb. The FRS samples were scanned at wavelengths ranging from 220 to 500 nm. The excitation wavelength was 280 nm. The slit width was set to 5.0 nm, and the proposed thickness of the quartz cuvette was 1.0 cm. The operational procedure was similar to that described previously [21]. The charge conveyance resistance between the cofactor in Hb and the conductive surface of the supporting electrode was probed using electrochemical

impedance spectrometry (EIS) and cyclic voltammetry (CV). The EIS spectra were registered under the following experimental conditions: a frequency of 0.1–10^5 Hz, an open circuit potential of 0.420 V, 5.0 mM $K_3Fe(CN)_6/K_4Fe(CN)_6$ + 0.1 M KCl as the supporting electrolyte, and a potential excitation amplitude of 5.0 mV. The steady CV curves were recorded in an O-free electrolyte without any substrate.

Electrochemical behavior of Hb@ZIF-67

The electrochemical measurements were performed using a conventional electrolysis cell with three electrodes. The working electrode was Hb@ZIF-67/GCE immersed in PBS. The electrolysis cell was attached to a cylinder containing N gas using a rubber tube. Multiple electrochemical techniques, including CV, differential pulse voltammetry (DPV), and linear scanning voltammetry, in combination with a rotating disk electrode and chronoamperometry (CA), were employed to analyze and determine the direct electron transfer mechanism and electrocatalytic efficacy of the Hb-based electrodes in reducing H_2O_2. The CV curves of the Hb-based electrode were recorded in an electrolyte without an electron mediator under steady-state conditions. The DPV curves were recorded using a step potential of 5 mV and a pulse gap of 0.05 s. The CA experiments were executed at an applied potential of –0.4 V. The current–time curve was obtained under normal pressure and room temperature (24.6 ± 0.7 °C) without any additional indication. The electrolyte with H_2O_2 concentration modulation in the CA experiments was prepared via the addition of 100.0 µL PBS with 5 mmol·L^{-1} H_2O_2 into the stock solution without H_2O_2 every 100 s. All the potentials in this article are relative to those of the normal hydrogen electrode. From the gap in the reduction current between the reference state (i.e., the electrolyte without H_2O_2) and the presence of a dissolved substrate under the limiting diffusion potential introduced earlier, the electrocatalytic performance in H_2O_2 reduction for the Hb-based electrode was estimated [19].

Results and discussion

Characterization and investigation of the morphology, structural traits, and physicochemical features of ZIF-67 with Hb attachment

The immobilization capacity of heme protein into ZIF-67 evaluated by GFAAS was 112.3 mg·g^{-1} calculated according to the method described in a previous report [23]. This value is much higher than that of Hb integration into ZIF-8 with atomic Zn as the central element (80.6 mg·g^{-1}) [17]. The difference in the protein accommodation capability between the two cases is attributable to the unique affinity of Co to the heme protein molecule and the promotion of Hb molecule formation by Co. The former assumption was validated by additional measurements of the Hb loading amount for enzyme carriers with the Co-complex as the main component. Thus, such Hb supporters with Co-complexes connected to redox hydrogels display relatively high enzyme immobilization capabilities (data not presented in the current manuscript). Furthermore, the unique electron distribution of Co^{2+} (half-filling state of the 3d orbit) with a positive charge should contribute to the higher loading capacity of Hb (electronegative state in a near-neutral electrolyte). The specific catalytic activity for H_2O_2 reduction of Hb incorporation into ZIF-67 was determined to be 0.74 U·mg^{-1}, which is slightly higher than that for heme protein entrapment into ZIF-8 (0.66 U·mg^{-1}) [24]. The improved catalytic activity of Hb immobilization onto ZIF-67 can be ascribed to the weaker impact of the competitive ligation between a metal element and a heteroatom in the ligand on the catalytic mechanism of immobilized Hb. The molar ratio of Hb detachment from ZIF-67 was estimated to be 36.1%, which is close to that of Hb desorption from Ag nanorods, as demonstrated previously (33.5%) [24]. This result can be attributed to the competitive complexation of Hb with ZIF-67, which is similar to the coordination of Ag with the surface amino acid residues on Hb. The results of additional experiments revealed that the N_2 adsorption–desorption isotherm should be imputed to a typical I class curve for rapid adsorption to reach the saturation status and wide pore size distribution for both ZIF-67 alone and the MOF with Hb attachment (Fig. S1 and Table S1). The results also suggest that only a small portion of Hb molecules could be stashed in the pores of the MOF material, reducing the specific surface area and pore capacity of ZIF-67 with Hb immobilization to a certain extent. Considering the footprint of a native Hb molecule (approximately 5.0–6.5 nm), the pores in the MOF material could not be blocked by the aggregation cluster of Hb molecules via the H bonding and hydrophobic–hydrophobic interaction. This characteristic also implies that the integrated heme molecules could not be completely inserted into the pores of the MOF material.

Figure 2 shows the SEM images of ZIF-67 alone (a) and ZIF-67 with Hb attachment (b). The secured morphology of ZIF alone shows a regular diamond dodecahedron shape and a uniform size of approximately 250 nm (inset in Fig. 2) as well as a clear edge in general. The morphology of ZIF-67 underwent a notable change after Hb attachment, with the original geometrical shape of the MOF material partially

Fig. 2 SEM images of ZIF-67 alone (**a**), inset graph: size distribution of as-prepared ZIF-67, ZIF-67 with Hb attachment (**b**) and the EDX-SEM image of nano-complex with Hb entrapment in combination with its element mapping image (**c**)

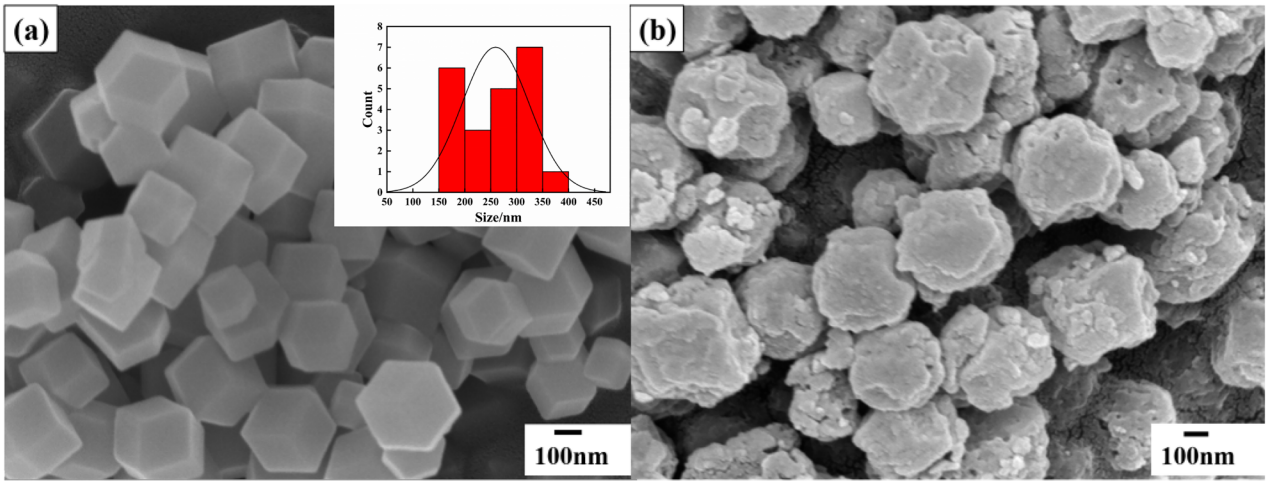

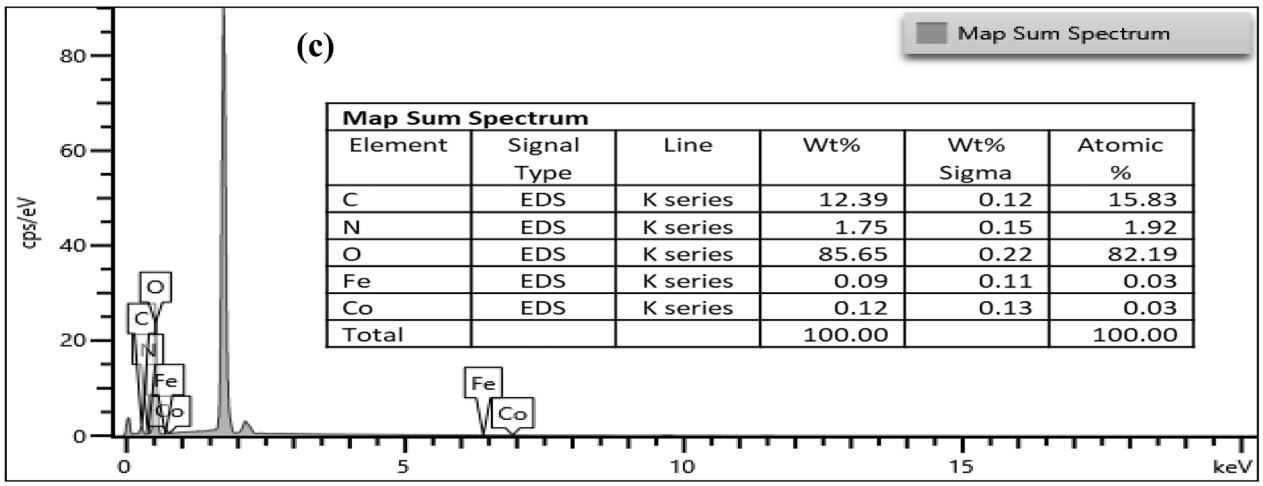

Map Sum Spectrum

Element	Signal Type	Line	Wt%	Wt% Sigma	Atomic %
C	EDS	K series	12.39	0.12	15.83
N	EDS	K series	1.75	0.15	1.92
O	EDS	K series	85.65	0.22	82.19
Fe	EDS	K series	0.09	0.11	0.03
Co	EDS	K series	0.12	0.13	0.03
Total			100.00		100.00

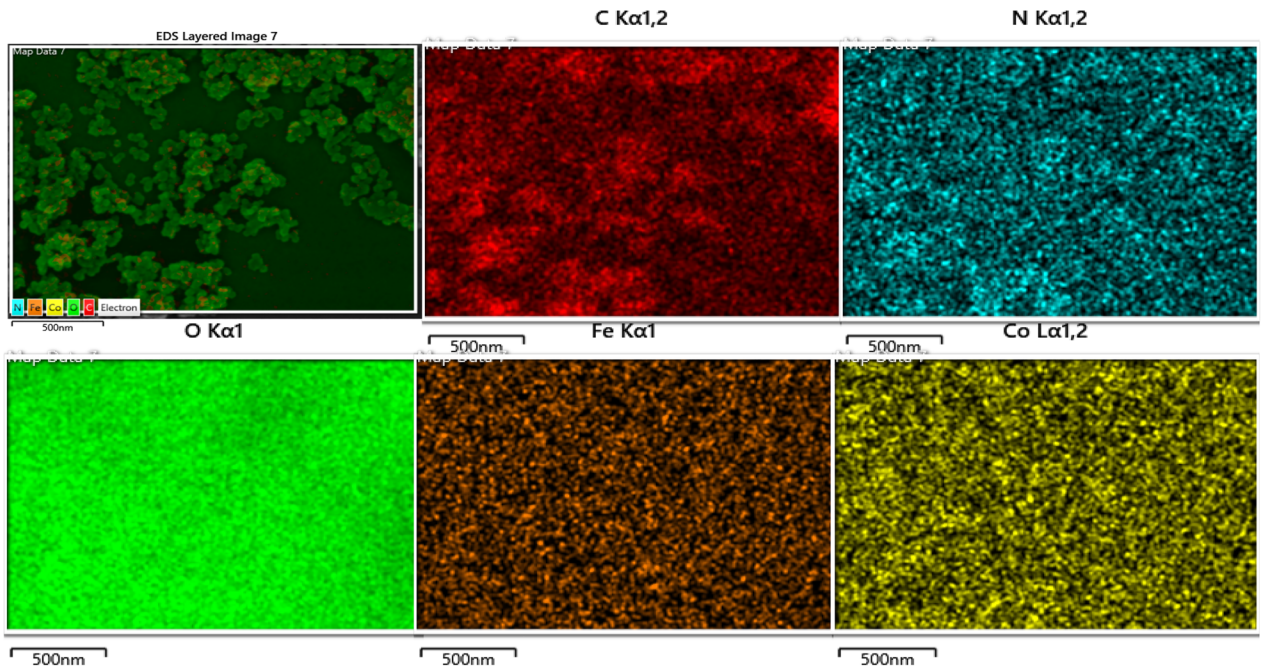

disappearing and the edges of the dodecahedron becoming obscure. These findings indicate that the segmental surface of the MOF material could be overcoated with heme protein molecules. Furthermore, smooth and planar layer-like structures are observed in Fig. 2b. The existence of a relatively oriented shape of the composite units can be ascribed to the oriented arrangement of some Hb molecules on ZIF-67, arising from the relatively weaker ligation between amino acid residues on the surface onto the surface of Hb and Co ions within ZIF-67. Some gigantic clusters comprising Hb aggregates can be identified in Fig. 2b. The presence of such structures indicates that most Hb molecules can be randomly distributed and stacked onto ZIF-67 via H bonding. The EDX-SEM images of the ZIF-67 nanocomplex with heme protein incorporation are illustrated in Fig. 2c. The analysis in Fig. 2c indicates the existence of diagnostic peaks for C, N, O, Fe, and Co. The small amount of Hb adsorbed on the surface of ZIF-67 can be attributed to the low-intensity characteristic Fe peaks. In addition, the elemental mapping image shows that the nanocomplex contains C, O, Fe, and Co atoms as its main components, along with heme protein entrapment. These characterization results strongly indicate that Hb molecules were successfully incorporated into ZIF-67.

The XPS spectra of the various constituent components (Co, C, N, O, and Fe) in ZIF-67 before and after Hb entrapment are presented in Fig. 3a–f, respectively. Figure 3a reveals that the diagnostic band for Fe 2p is present in the XPS spectrum of ZIF-67 with Hb entrapment. This result indicates the successful incorporation of heme protein into the ZIF material. This assumption is supported by the comparison of Fig. 3a with Fig. 3f of Fe 2p in ZIFs with Hb attachment and free Hb. It means that two strong bands at 716.0 eV for Fe 2p1/2 and 707.0 eV for Fe 2p3/2 are recognized in the XPS spectrum of native Hb. Both peaks indicate the existence of Fe in the oxidation state of Fe^{3+} and the reduction state of Fe^{2+} within the Hb molecule in a specific microchemical environment (i.e., the given amino acid ligands near the heme site of Hb). The disappearance of the latter reveals the oxidation of Fe within Hb after its integration into the ZIF material in the presence of a relatively weak complexation of Co in ZIF-67 with the surface amino acid residues of Hb. The presence of Fe 2p can only be considered as part of the proof chain to consolidate the successful integration of Hb into ZIF. The identification of the Fe 2p peak and the variation of this signal location after Hb attachment onto ZIF-67 reveal the change in the oxidation state of Fe from the mutual interaction between Hb and ZIF-67. No signal for the existence of Fe can be discerned in the XPS spectrum of ZIF-67 alone, and the origin of the signal for Fe in the spectrum of ZIF-67 with Hb anchoring is attributed to the introduction of Hb with the Fe-porphyrin complex as the electroactive site in Hb. Furthermore, multiple experimental results support the conclusion that Hb can be successfully immobilized onto ZIF-67. The results from the FTIR measurements, CD tests, FRS determination, and UV–Vis experiment support the assumption that the heme protein can be favorably integrated into the enzyme matrix, as discussed in the previous sections of the current submission. Constant locations for Co 2p1/2 (796.8 eV) and Co 2p3/2 (781.5 eV) were detected after the integration of Hb into ZIF-67. This result implies that competitive complexation between heteroatoms within the imidazole ring and the heme site in Hb does not have a remarkable effect on the oxidation–reduction status of Co in the MOF material. The difference between the 2p1/2 and 2p3/2 peaks of Co (15.3 eV) indicates that the transformation from the oxidation state to the reduction state can be attributed to the switching of the valence status between Co (III) and Co (II).

The XPS spectrum of Co 2p illustrated in Fig. 3b indicates a nearly identical energy gap between the Co 2p3/2 and Co 2p1/2 of ZIF-67 before and after Hb immobilization. The difference between the two cases is the slight positive shift of such bands to high binding energy and the apparent enhancement in the intensity of these bands after Hb incorporation into the ZIFs. This result is attributed to the competitive ligation of Co in the ZIFs with heteroatoms in the amino acid residues on the surface of the heme protein molecules. The invariable locations of the featured peaks for C, N, and O in both the ZIFs and ZIF-67 with Hb accommodation are shown in Fig. 3c–e. These results indicate that the reciprocal interactions between Hb and ZIF-67 do not have a serious effect on the chemical microenvironment of the backbone as ligands within the ZIFs.

The XRD spectra of ZIF-67 alone and the complex of MOF material with Hb attachment are shown in Fig. 4. Only a single isolated, wide, and weak peak located at $2\theta = 19.3°$ is evident in the XRD spectrum of native Hb [25], indicating that the molecular structure of the free heme protein lacks well-ordered units. A series of diffraction signals at 7.5°, 10.5°, 12.8°, 14.8°, 16.6°, 18.1°, 22.2°, 24.6°, 25.6°, 26.8°, 29.7°, 30.7°, 31.7°, and 32.6° is apparent in the XRD spectrum of ZIF-67 alone. These peaks can be attributed to the existence of the following diagnostic crystalline surfaces: (0 1 1), (0 0 2), (1 1 2), (0 2 2), (0 1 3), (2 2 2), (1 1 4), (2 3 3), (2 2 4), (1 3 4), (0 4 4), (3 3 4), (2 4 4), and (2 3 5) with variable interlayer gaps of 1.179, 0.842, 0.692, 0.599, 0.543, 0.490, 0.400, 0.362, 0.348, 0.333, 0.301, 0.291, 0.282, and 0.275 nm. This result is similar to those reported previously [26, 27]. This finding also indicates the successful preparation of pure ZIF-67 crystals with a high degree of crystallization. No notable variations in the locations of the diffraction peaks of ZIF-67 are evident after Hb attachment. The mutual interaction between Hb and ZIF-67 did not have a serious effect on the original crystal phase trait of ZIF-67, and the inherent configuration of the cofactor

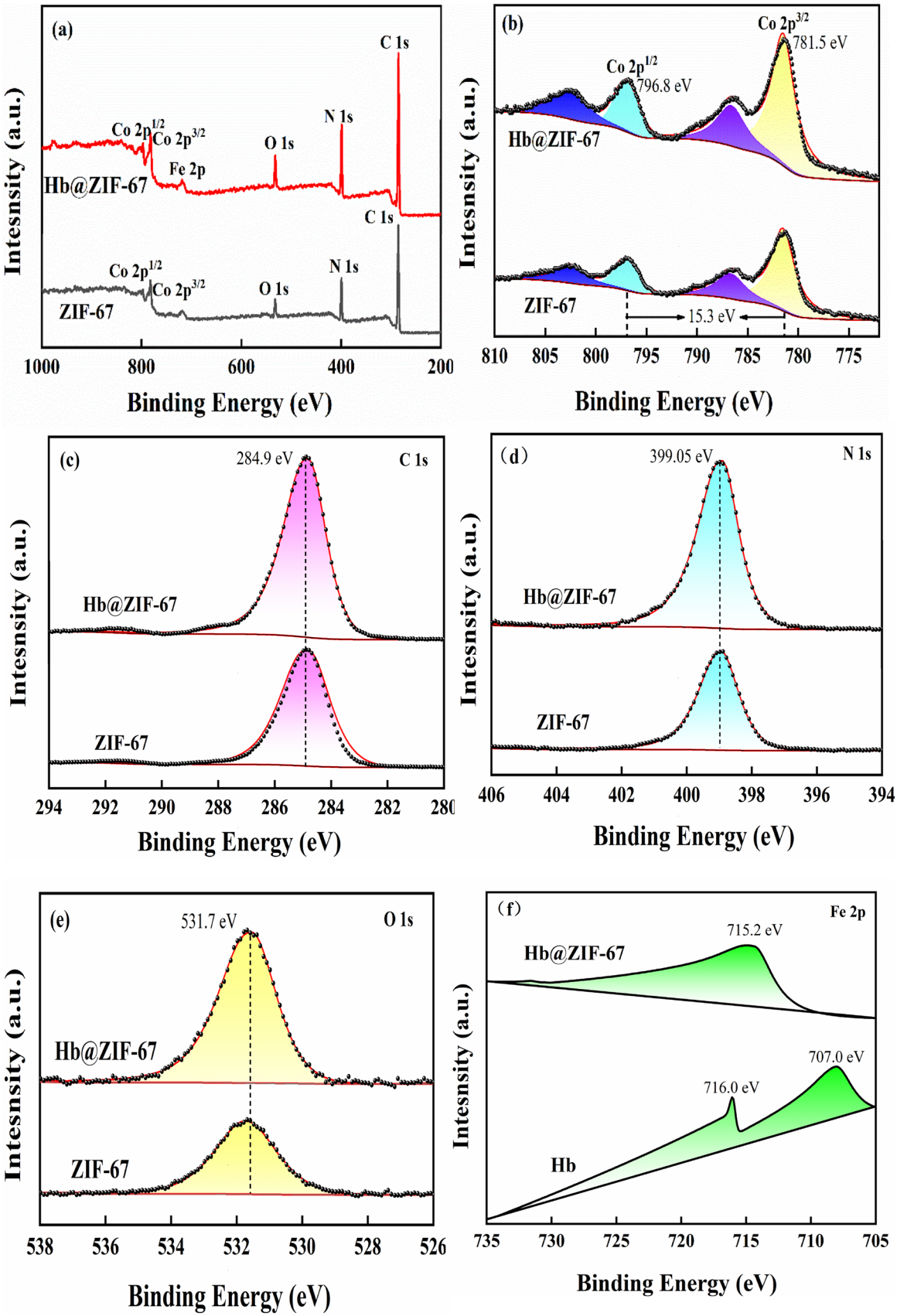

Fig. 3 XPS spectra of different components in ZIF-67 and ZIFs with Hb accommodation: all elements (**a**), Co (**b**), C (**c**), N (**d**), O (**e**), and Fe (**f**)

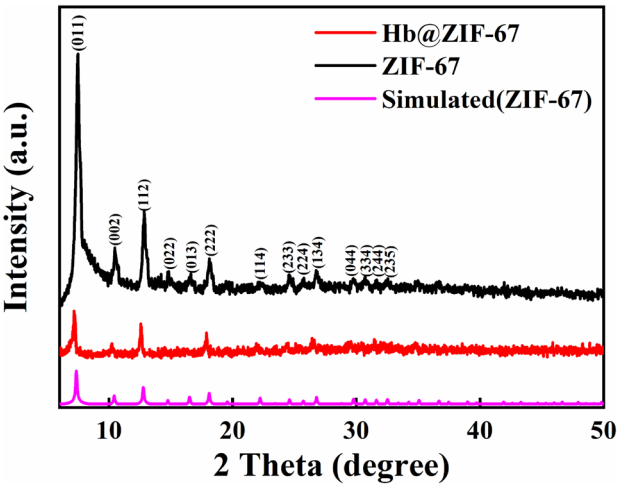

Fig. 4 XRD spectra of ZIF-67 alone and the complex of MOF material with Hb

in Hb remained intact to an extraordinary extent. This phenomenon indicates that the insertion of Hb molecules into the hollow holes of ZIF-67 in the absence of a remarkable left shift in the features of the ZIF-67 crystal structure is not possible. This characteristic also suggests the existence of a weak interaction between ZIF-67 and the integrated Hb. Otherwise, novel and distinct diffraction signals or the disappearance of some diagnostic signals can be observed [25] in the presence of a strong interaction between the heme protein and the enzyme support.

Figure 5 shows the FTIR spectra of pure Hb, ZIF-67, and the MOF material with heme protein attachment. Infrared peaks for the secondary structures of native heme protein molecules situated at 1661 and 1543 cm^{-1} are evident in the spectrum of free Hb. The former peak can be ascribed to the presence of the amide I band for the C=O stretching vibration, whereas the latter can be attributed to the existence of the amide II band for the C–N stretching vibration and N–H in-plane bending vibration [28–30]. The notable band of Co–N stretching vibration at 422 cm^{-1} can be identified in the spectrum of pristine ZIF-67. This result confirms the successful coordination of Co with the heteroatoms in the imidazolyl ring. The two bands at 757 and 1578 cm^{-1} can be attributed to the out-of-plane bending vibration of C–H and C=N stretching vibration, respectively. The peak at 1303 cm^{-1} can be ascribed to the stretching vibration of the imidazole backbone. The band at 991 cm^{-1} should be associated with C–N bending vibration, and that at 1141 cm^{-1} is attributable to the presence of C–N stretching vibration. The two bonds at 1421 and 2935 cm^{-1} can be attributed to the stretching vibrations of the hetero-aromatic molecule backbone and C–H in the hetero-aromatic ring, respectively [1, 31–34]. The identical absorption peak at 1661 cm^{-1} can be observed in the spectrum of ZIF-67 with Hb accommodation. An apparent positive shift to a higher wave number for the amide II band (1570 cm^{-1}) can be detected in the case of ZIF-67 after Hb attachment. This result indicates competitive ligation between the metal elements in Hb or ZIF-67 and heteroatoms within the surface amino acid residues or imidazole rings, as illustrated elsewhere [19]. To a certain extent, distinct ligation had a remarkable effect on the physicochemical idiosyncrasies of the integrated Hb molecules.

The UV–Vis spectra of pristine Hb powder (a), the ZIF-67 solid phase (b), and ZIF-67 with Hb incorporation (c) are shown in Fig. 6. An intense adsorption peak located at ~ 225 nm is common among these three cases. This signal can be associated with the huge π electron conjugation systems in these systems (i.e., hydrophobic sites within the

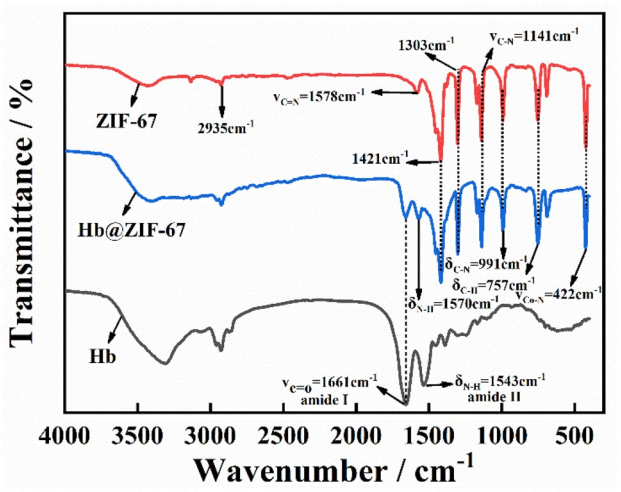

Fig. 5 FTIR spectra of aboriginal Hb, ZIF-67 alone and MOF material with heme protein attachment

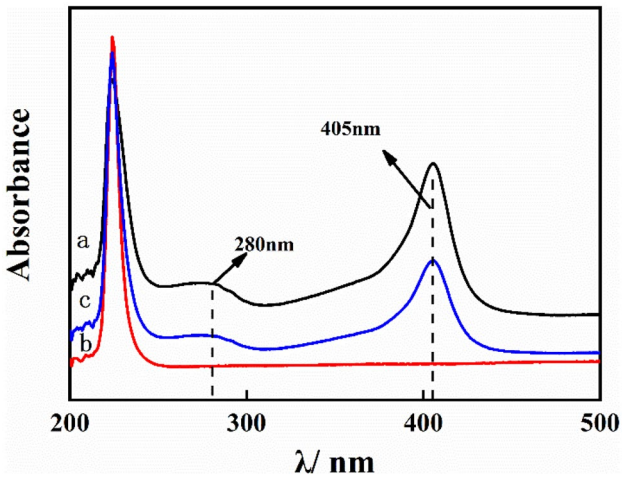

Fig. 6 UV–Vis spectra of pristine Hb powder (**a**), ZIF-67 solid phase (**b**), and ZIF-67 with Hb incorporation (**c**)

Hb molecule and hetero-aromatic ring as ligands in ZIF-67). The common peak can be attributed to the π–π* electron transition in the systems mentioned previously. A wide side absorption peak at ~ 280 nm can be detected in both the native heme protein and when Hb is attached onto ZIF-67. This signal should be related to a π–π* or n–π* electron transition for the chromophores in the heme protein [28, 35]. The common band at 405 nm (i.e., the Soret absorption band) in both cases (anchoring of free Hb and ZIF-67 with Hb) can be attributed to the d–d electron transition of the Fe–porphyrin complex [36]. The identical peak for both systems suggests that the reciprocal interactions, including the hydrogen bond and weak ligations between the elements of ZIF-67 and Hb, did not have a prominent impact on the intrinsic configuration of the heme site. Additional UV–Vis measurements confirmed that the presence of ZIF-67 contributed to the intact configuration of the electroactive sites within Hb. This characteristic indicates that the coalescence of ZIF-67 with some nanomaterials (e.g., graphene oxide and Ag nanoparticles) maintains the inherent configuration of the active sites within Hb. Different MOF materials (e.g., ZIF-8) do not produce the same effect [24].

Figure 7 shows the CD spectra of ZIF-67 alone, ZIF-67 with Hb attachment, and pristine Hb. Two consecutive, distinct, and negative absorption peaks located at 209 and 221 nm are evident in the spectrum of free Hb. The two featuring bands should be attributed to the existence of π–π* and n–π* transitions of the α-helical peptide bond in Hb. No distinct positive or negative absorption bands can be observed in the spectrum of ZIF-67. This finding reveals the absence of a hydrophobic structure (i.e., α-helix, β-sheet, and β-corner structure) within the as-prepared MOF material (ZIF-67), resulting from the complete overlapping of ZIF-67 with entrapped Hb with plenty of hydrophilic groups, such as carboxylic and amino groups, as shown in the zoomed-in graph in Fig. 6. The current system is distinct from the case introduced elsewhere [17]. The distinct spectrum of ZIF-67 with entrapped Hb is shown in Fig. 7, which reveals an idiosyncratic peak at 209 nm and a narrow peak at 221 nm after Hb attachment onto ZIF-67. These results indicate that the orderliness of native heme protein after enzyme integration into ZIF-67 can be crippled, and the hydrophilicity of immobilized Hb can be improved to a certain extent by the synergistic effect of competitive complexation and hydrogen bond between Hb and the elements of ZIF-67, as in the previous analysis. The disappearance of the diagnostic negative absorption band at 209 nm can be attributed to intermolecular or intramolecular interactions, such as hydrogen bond between immobilized Hb molecules and the relatively weak competitive complexation between Co ions within ZIF-67 and the amino acid residues of the incorporated Hb. Such interactions can cause a change in the configuration of the α-helix structure.

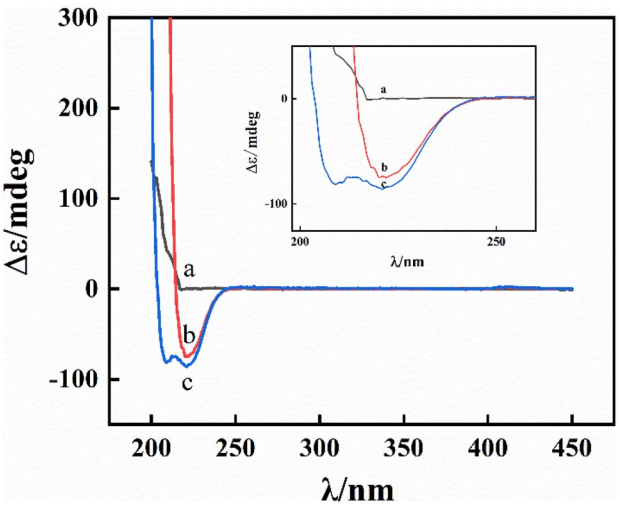

Fig. 7 CD spectra of ZIF-67 dispersed phase (**a**), MOF material with discrete Hb incorporation (**b**) and dissolved Hb (**c**)

The FRS spectra for several dispersed phases with constant heme protein content of 0.25 mg·mL^{-1} and different contents of ZIF-67 are presented in Fig. 8. The plot of F_0/F against the fluorescence quenching agent content is also exhibited in the inset of Fig. 8. The diagnostic band at ~ 330 nm for the presence of surface amino acid residues such as Tyr and Trp can be identified in the spectrum of native Hb alone. A moderate decrease in the strength of the

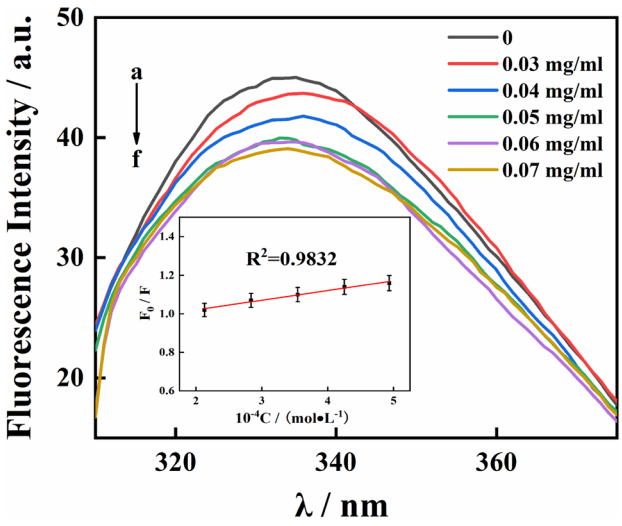

Fig. 8 Fluorescence spectra of the mixtures composed of constant consistency of Hb at 0. 25 mg·ml^{-1} and variable contents of ZIF-67, its inset: the dependence plot of F_0/F on the content of fluorescence quenching reagent, F_0 and F indicating fluorescence intensity of heme protein in the absence of quenching reagent and that of Hb in the presence of quenching reagent at different content levels, respectively. curve a ~ f indicating the different content levels of ZIF-67: 0, 0.03, 0.04, 0.05, 0.06, 0.07 mg·ml^{-1}

idiosyncratic peaks can be detected after the introduction of ZIF-67. The decrease in the intensity of the featured band of free Hb is proportional to the increase in ZIF-67 content, as shown in Fig. 8. No extra fluorescence emission band can be observed after the addition of ZIF-67 to the system. This finding indicates that the presence of novel intermediate species with distinct fluorescence features is not possible [37]. The quenching rate constant of the fluorescence (K_q) can be extrapolated to be 4.97×10^{10} L· (mol·s)$^{-1}$ from the slope of the plot in the inset of Fig. 8. This value is slightly higher than the thresholds of most fluorescence quenchers to biomacromolecules (2.0×10^{10} L· (mol·s)$^{-1}$). The extinction of the fluorescence emission band can be attributed to a typical mode of static fluorescence quenching via the combination of Hb and ZIF-67. Further, the binding sites of Hb with ZIF-67 and the binding constant of Hb in combination with the MOF material can be estimated to be 2 and 9.3×10^{6} L·mol^{-1} from the slope and intercept of the dependence plot of lg[(F_0–F)/F] versus the level of fluorescence quenching reagent (data not provided), respectively. The calculation equation was introduced in a previous study [38]. The combined strength of Hb with ZIF-67 was weaker than those in other similar cases [21] (i.e., protein in complexation with an organic dye molecule: 3.8×10^{7} L·mol^{-1}). This characteristic suggests that the impact of competitive coordination between Hb and ZIF-67 on the spectroscopic and electrochemical behaviors of immobilized Hb is subordinate.

The EIS spectra and corresponding CVs of the bare GCE, GCE over-coated by ZIF-67, and supporting electrode modified by a thin membrane of ZIF-67 with Hb anchoring in a PBS solution containing $K_3Fe(CN)_6/K_4Fe(CN)_6$ + KCl are shown in Fig. 9a and b, respectively. The diameter of the semicircle for the load impedance transfer of the bare GCE is the smallest among the three cases owing to its superior conductivity. The impedance of the GCE capped by ZIF-67 is remarkably enhanced compared to that of the bare GCE owing to the introduction of the MOF material with inferior conductivity and undesirable electrochemical activity. Accordingly, the redox potential gap for the electroactive species in PBS and the redox current intensity of the GCE over-coated with ZIF-67 are widened and attenuated, respectively. The resistance to electron transport for ZIF-67 with Hb accommodation is substantially higher than that for ZIF-67. Simultaneously, the redox band featuring the electrochemical probing species considerably diminishes, and the shape of the redox peak can be distorted to a great extent. These results can be attributed to the existence of an insulating protein backbone and the competitive complexation of $K_3Fe(CN)_6/K_4Fe(CN)_6$ with Hb. A higher electron transfer resistance can be considered deleterious for achieving Hb-induced electrocatalysis. In most cases, the enhanced resistance in electron shuttles can be attributed to redox protein integration into a specific enzyme carrier (i.e., nano-material, conductive polymer, or MOF material). The relationship between the increased electron conveyance resistance and the loss of electro-catalytic efficiency is not affirmative in many cases, as illustrated previously [24]. The influence of the mutual interaction between the redox protein and elements of the enzyme support on the configuration of the cofactor within the redox enzyme molecule contributes to the maintenance of the inherent electrocatalytic effect of immobilized redox protein molecules, as demonstrated in previous studies [17, 18, 24]. The latter can be confirmed by FRS measurements, as demonstrated elsewhere [17]. This assumption is consistent with previous analyses and deductions. These results also suggest a relatively weak interaction between Hb and ZIF-67, which also contributes to the desirable catalytic efficiency of the immobilized Hb. The relative interaction between the elements of the enzyme carrier and the redox protein protects the inherent configuration of the enzyme molecule from external interference.

Direct electrochemistry and electrocatalysis on H_2O_2 reduction for Hb@ZIF-67/GCE

Figure 10 shows the CV curves of static ZIF-67/GCE and Hb@ZIF-67/GCE in the absence of O and neutral PBS without an electron mediator. No distinct redox band can be

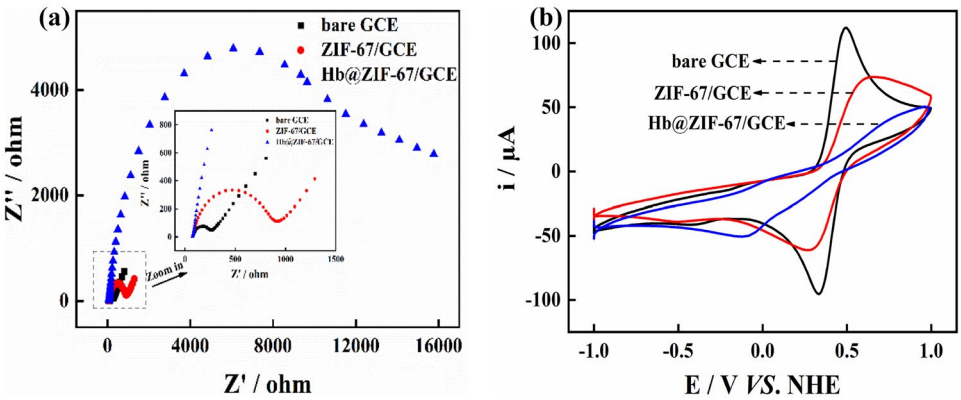

Fig. 9 EIS spectra (**a**) and corresponding CV curves (**b**) of bare GCE, supporting electrode over-coated by MOF material and Hb@ZIF-67 /GCE in PBS with 2.5 mM $K_3Fe(CN)_6$ + 2.5 mM $K_4Fe(CN)_6$ + 0.1 M KCl

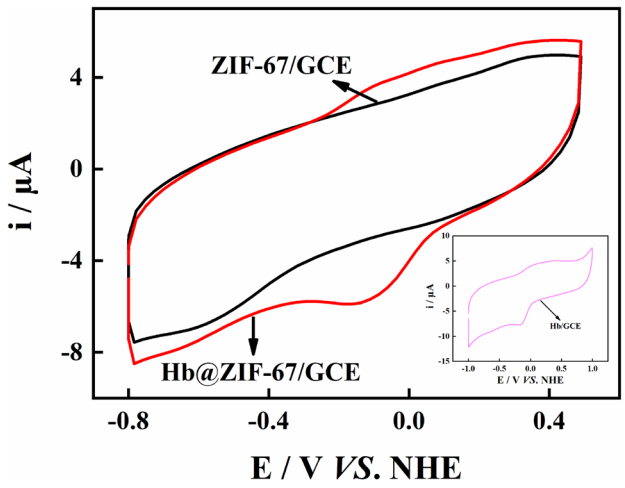

Fig. 10 CV curves of static ZIF-67/GC and Hb@ZIF-67/GC in oxygen-free and neutral PBS without electron mediator recorded at the scanning rate of 0.2 V·s^{-1}

recognized in the CV of ZIF-67/GCE in the electrolyte. The inset in Fig. 10 shows the CV curve of the GCE overcoated with the CTS membrane with Hb entrapment in the same electrolyte. These results revealed that the presence of electroactive groups on ZIF-67 can be ignored. Only a pair of weak redox peaks with inferior reversibility ($I_{p,c}/I_{p,a} > 2$) can be identified at ~ −0.14 V with the oxidization and reduction peak potential gap of 24.3 mV. The redox bands of the Hb-based electrode have a mean potential similar to the formal potential of the cofactor in native Hb [39]. The difference in the formal potential between the integrated and original Hb (the inset graph in Fig. 10) can be attributed to the different chemical microenvironments in the two cases. Such electrochemical signals should be attributed to the redox process of Hb integration into ZIF-67, and the difference between the two systems can be attributed to the variation between the microenvironments of pristine and immobilized Hb. Furthermore, the mutual interaction between Hb and ZIF-67 contributes to the difference between the mean potentials in the two cases. The formal potential and reversibility in the redox process for various processes for the various Hb-based electrodes, including the as-prepared electrode based on Hb incorporation into ZIF-67, are compared in Table 1. The oxidized and reduced states of Fe in Hb are

Table 1 The comparison in direct electrochemical behavior for different Hb based electrodes including Hb@ZIF-67/GCE

Modified electrodes	Formal potential	$I_{p,a}/I_{p,c}$	Refs
Hb@ZIF-8/GCE	−0.154 V	1.1	[17]
Hb/CdS@TiO_2/GCE	0.125 V	1.6	[18]
Hb/ZIF-8@Ag-CTS/GCE	0.114 V	1	[24]
Hb@ZIF-67/GCE	0.14 V	2	This work

Fe^{III} and Fe^{II}, respectively, according to the descriptions of native Hb in previous works [17, 18, 24, 39]. In addition, the XPS measurements provide evidence to validate the existence of $Fe^{3+/2+}$. Two strong bands at 716.0 eV for Fe 2p3/2 and 707.0 eV for Fe 2p1/2 are evident in the XPS spectrum of native Hb. The disappearance of the latter indicates the oxidation of Fe within Hb after its integration into the ZIF material.

Finally, the surface coverage of electrically wired Hb can be estimated using the known surface-active area and amount of Hb molecules that can achieve direct electron transfer. The previous parameter can be obtained using a method described elsewhere [40]. The latter can be deduced from the quotient of the mean value of redox peak integration to the product of the electron numbers involved in the redox process on the Hb-based electrode (n) ($n = 4$, as in the previous analysis [17]), the Faraday constant, and the potential sweeping rate. The electrically wired Hb amount was accordingly determined to be 9.6×10^{-11} mol·cm^{-2}. This value is lower than that of a similar system (i.e., ZIF-8 with Zn^{2+} as the central ion) [17] and can be attributed to the discrepancy between the Zn complex and Co composite in a complicated environment (i.e., the distinct outer electron distribution configuration of Co from Zn, as discussed earlier).

Figure 11 shows the steady i–E curves of Hb@ZIF-67/GCE in deaerated PBS recorded at different potential sweeping rates. The peak currents for oxidation and reduction are plotted linearly against the square root of the potential scanning velocity, in the inset of Fig. 11. Figure 11 shows that the oxidation and reduction peaks of the Hb-based electrode are not significantly affected by an

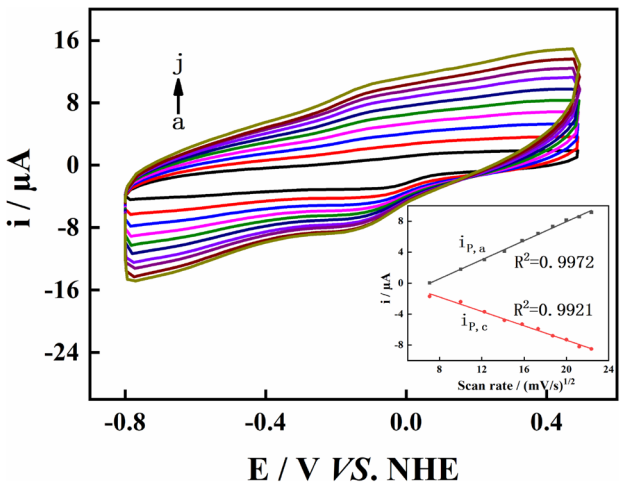

Fig. 11 CV curves of static Hb-based electrode in neutral and oxygen-free PBS registered at variable rates of potential scanning and its inset graph: the linear-fitting plots of redox peak currents versus square roots of potential sweeping rates (curves from a to j indicating 50, 100, 150, 200, 250, 300, 350, 400, 450, and 500 mV s^{-1})

increase in the potential scanning velocity. The oxidation and reduction currents increase with increasing sweep velocity. Within the scanning range of the test potential, the linear relationship between redox currents and the square roots of the potential sweep rate is maintained, as illustrated in the inset of Fig. 11. The ratio of the oxidation current versus the reduction current is close to 1.0 (~ 1.08 under a scanning velocity of 500.0 $mV{\cdot}s^{-1}$) under a strong electrochemical stimulus. This finding suggests the improved reversibility of redox processes involving Hb. Additional electrochemical experiments support the view that the presence of Co^{2+} promotes the charge transport efficiency of graphene oxide and magnetic nanoparticle complexes with Hb integration in a solution containing Co^{2+}. This characteristic indicates that the intensity of the redox bands can be augmented by the narrow potential gap between the oxidation and reduction peaks (data not provided). The result is similar for the C nanotube–polypyrrole composite with Hb immobilization immersion into an electrolyte containing Co^{2+}. The shape of the *i–E* curve of the Hb-based electrode in an electrolyte containing Co ions is close to that of ZIF-67 with an Hb-based electrode. This result contradicts that for Hb in combination with ZIF-8 reported previously [17]. The experimental results suggest that the typical thin-film control mode is responsible for the quasi-reversible redox process of the Hb-based electrode in the current study [40]. The apparent diffusion coefficient (D_a) for electrically wired Hb binding to ZIF-67 can be calculated to be 6.7×10^{-6} $cm^2{\cdot}s^{-1}$, according to the equation demonstrated in another report [41], from the slope of the linear fit curve in Fig. 10. The definition presented elsewhere provides the normalized heterogeneous electron shuttle rate (k_{het}) for a Hb-based electrode [19]. The kinetic parameter was determined to be 0.1 s^{-1} by considering the following important variables as preconditions: the dependence index to the redox peak potential gap (Ψ, which can be set to 0.22 under a high potential scanning rate of 2.0 $V{\cdot}s^{-1}$), the efficient thickness of the thin film (δ, which can be estimated to be 0.054 cm), D_a (unit: $cm^2{\cdot}s^{-1}$), and *n*, as discussed previously.

The DPV curves of static Hb@ZIF-67/GCE in O/electron relay-free and neutral electrolytes, obtained under modulated impulse heights for both potential scanning directions (negative and positive sweeping), are shown in Fig. 12 a and b, respectively. Two isolated reduction peaks can be detected in the negative potential scanning course, as demonstrated in Fig. 12a. The reduction peak location at a relatively negative potential (~ − 0.74 V) remains stable with increasing pulse height. The presence of this electrochemical signal can be attributed to the electro-reduction of O_2 adsorption onto ZIF-67. This result is similar to that reported previously [19]. Another reduction at a positive potential can be ascribed to the reduction reaction at the heme site of Hb in its native form for a slight shift in its location in comparison to that of the original Hb. Two consecutive oxidation bands are evident in the positive potential-sweeping process (Fig. 12b). A similar constant oxidation peak location can be observed at a relatively negative potential for the cofactor in free Hb. Another peak can be observed at a more positive potential. A slight shift in the secondary oxidation peak with increasing pulse height can be detected in Fig. 12b, and the existence of such an oxidation band can be attributed to the electron exportation process for the heme site in complexation with ZIF-67. Notably, two consecutive oxidation bands amalgamate into a single wide oxidation peak located at a relatively negative potential. These results indicate that the electrochemical reaction can be dominated by the heme site in the free state within Hb and that the competitive coordination of Hb with ZIF-67 does not have a significant effect on the electron conveyance route of the integrated Hb. In the current manuscript, Hb in the free state refers to the partial integration of Hb molecules into ZIF-67, which has a configuration similar to that of native Hb according to the UV–Vis measurement results and FRS tests. Some of the immobilized Hb molecules exhibited a catalytic effect on substrate reduction, similar to the original heme protein. The previous analysis of the electrochemical behavior of Hb-based electrodes showed that the electron shuttle mechanism is distinct from those in the mode of the surface confinement

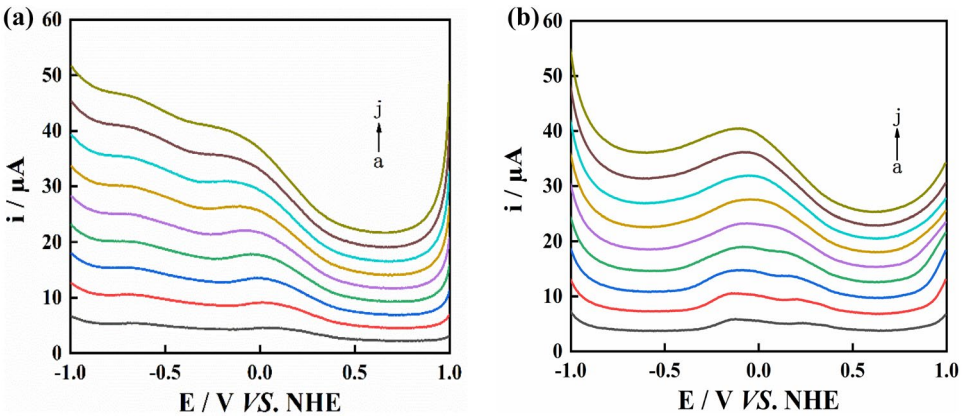

Fig. 12 DPV curves of Hb@ZIF-67/GCE in nitrogen-bubbling PBS at neutral pH recorded at different pulse widths for negative potential scanning (**a**) and positive potential scanning (**b**)

pattern for electro-active group immobilization onto a specific supporter. This finding implies that the electro-active sites within Hb@ZIF-67 perform charge transfer in a swaying or hopping mode, similar to the electron shuttle chain with desirable retractility.

The CVs of the quiescent Hb@ZIF-67/GCE in electron relay and neutral PBS with pH regulation are shown in Fig. 13. The inset in Fig. 13 shows a linear fit of the mean redox peak potential for the Hb-based electrode versus the pH of the buffer solution. According to the Nernst equation, the mean value of the redox wave potential for Hb attachment onto ZIF-67 shifts toward a negative potential with increasing pH of the PBS. The ratio of n to x (H^+ involvement in the redox process of Hb entrapment onto ZIF-67) can be extrapolated to be 2:1 from the slope for the linear-fitting plot in the inset of Fig. 13 (− 28.0 mV/pH). Usually, four electrons are involved in the electrochemical process of the original Hb. This characteristic indicates that two protons are included in the electrochemical reaction that occurs on the Hb-based electrode.

Figure 14a and b show the CVs of quiescent Hb@ZIF-67/GCE and the reference electrode, ZIF-67/GCE, in neutral and N_2-bubbling PBS containing different H_2O_2 concentrations. Figure 14a demonstrates that the sharp increase in the electroreduction current at a potential more negative than ~ − 80 mV and the augmentation magnitude are enhanced with increasing dissolved H_2O_2 consistency. The onset potential of the Hb-induced electrocatalysis can easily be deduced to be ~ 112 mV. Further, the Hb-based electrode is evidently sensitive to the content of dissolved H_2O_2 in the electrolyte. A similar result is not observed for the case of the ZIF-67-based electrode, as demonstrated in Fig. 14b.

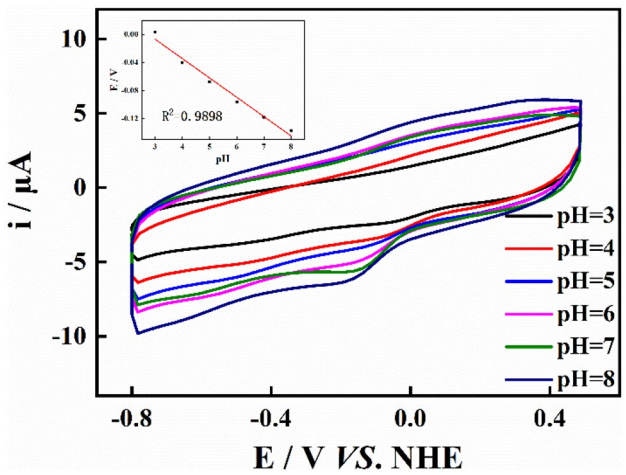

Fig. 13 CV curves of the quiescent Hb-based electrode in oxygen free PBS with pH regulation recorded at a scanning rate of 200.0 mV s^{-1} and the relevant linear-fitting dependence plot of reduction peak potential for Hb@ZIF-67/GCE on pH value of buffer solution

No remarkable elevation in the electroreduction current at a negative potential can be identified. Notably, the difference in the reduction current response at high substrate concentrations can be reduced. This characteristic can be attributed to the chemical reaction between H_2O_2 and Co in ZIF-67. The extra O concentration measured using the Clark O electrode, as described in an earlier report [42], supports this assumption. This result means that the concentration of dissolved O molecules increases by ~ 2.4% after the ZIF-67-based electrode is incubated in air-saturated PBS with a H_2O_2 consistency of 1.5×10^{-5} mol·L^{-3} for 2 h. The response of the electrocatalytic effect on H_2O_2 reduction for ZIF-67 with Hb integration is higher than that for ZIF-67 alone in the presence of the substrate. This finding confirms the assumption that efficient direct electron transfer can be accomplished between the heme site in the Hb molecule and the conductive surface of the ZIF-67-based electrode. This result also implies that the immobilized Hb molecules catalyze substrate reduction efficiently, as illustrated in previous studies [5, 10, 17, 18, 24, 25]. This conclusion cannot be considered contradictory to the experimental results shown in Fig. 9. This deduction is also consistent with the UV–Vis measurements, CD experiments, and FRS tests. The current response of the Hb-based electrode is much lower than that of ZIF-67-based electrode in the presence of 2.5 mM $K_3Fe(CN)_6$ + 2.5 mM $K_4Fe(CN)_6$ as the electrochemical probing species (Fig. 9b). This result is consistent with the analysis of the EIS spectra in Fig. 9a. The sensitivity of the Hb-based electrode to dissolved O molecules, the Michaelis constant (K_M), and the low detection limitation (*LOD*) can be determined to be 4.3×10^{-4} A·L·mol^{-1}, 205 μM, and 9.5×10^{-3} mM, respectively, using the methods described elsewhere [21, 25]. The corresponding parameters of the ZIF-67-based electrode can be evaluated to be 4.6×10^{-4} A·L·mol^{-1}, 221 μM, and 9.8×10^{-3} mM, respectively. Comparison of the measurement results obtained in these two cases indicates that the introduction of Hb into ZIF-67 enhances the electrocatalytic efficacy for H_2O_2 reduction with slightly improved affinity. However, both cases show similar sensitivities to the substrate and detection limits for the unique surface characteristics of ZIFs to restrain substrate diffusion.

The CA curves of Hb@ZIF-67/GCE in electron-mediator-free and magnetically stirred PBS with H_2O_2 consistency levels under control at different time intervals are illustrated in Fig. 14c. The corresponding linear-fitting plot of the steady electroreduction current against the substrate consistency is shown in the inset in Fig. 14c. The rapid achievement of the steady-current plateau region for the Hb-based electrode is confirmed by Fig. 14c. A relatively stable current over time can be maintained until the next addition of PBS to the dissolved substrate. This result indicates that the as-prepared Hb@ZIF-67/GCE is sensitive to the presence of H_2O_2 in the

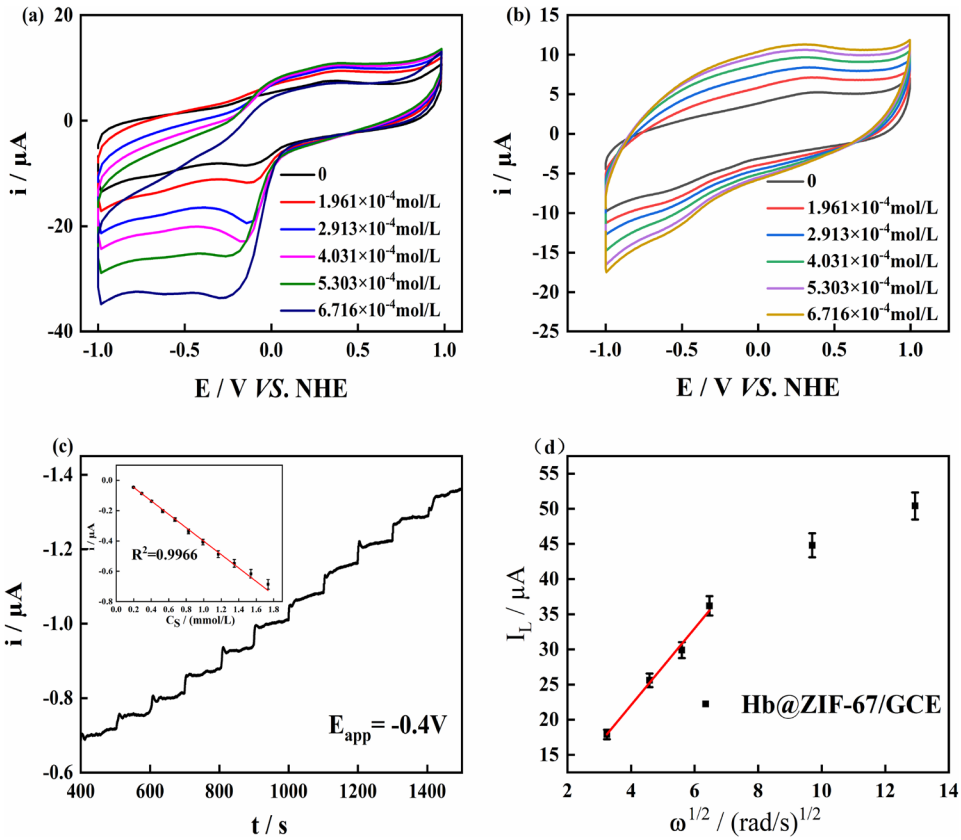

Fig. 14 CVs of quiescent Hb@ZIF-67/GCE (**a**) and reference electrode: ZIF-67/GCE (**b**) in neutral and N_2 bubbling PBS containing different H_2O_2 concentration levels recorded at the potential sweeping rate of 200.0 mV·s^{-1}; CA curve of Hb@ZIF-67/GCE in electron mediator-free and magnetic stirring PBS with consistency levels of hydrogen peroxide under controlling at different time intervals registered under the stable applied potential (**c**). The dependence plot of the Levich current for Hb-based electrode in neutral and electron relay-free PBS with 1.5×10^{-5} mol·L^{-1} H_2O_2 recorded at the potential scanning rate of 200.0 mV·s^{-1} against the square root of the electrode rotating rate (**d**)

electrolyte. This finding also suggests that the dynamics of substrate attachment onto ZIF-67 with Hb anchoring can be compared to that of H_2O_2 transformation. A desirable linear relationship between the electroreduction current and the concentration of the dissolved substrate is maintained within the testing substrate consistency window. The sensitivity and detection limitation of the as-prepared Hb-based electrode to the substrate are determined to be 4.4×10^{-4} A·L·mol^{-1} and 8.9×10^{-3} mmol·L^{-1}, respectively, as described elsewhere [43, 44]. The limiting electrocatalytic current for enzyme-involved H_2O_2 reduction (i_{cat}^{lim}) and K_M can be extrapolated to be 2.4 μA and 194.0 μM from the slope and intercept of the reciprocal linear-fitting plot, respectively.

Hence, the normalized apparent rate constant of Hb-induced electrocatalysis of H_2O_2 reduction can be estimated to be 4.3 s^{-1}, according to a previously introduced method [19]. This parameter is also known as the normalized substrate turnover frequency of H_2O_2 attachment to ZIF-67 with Hb accommodation (k_T). The disadvantages in the electrocatalytic and electrochemical sensing performance of immobilized Hb result from the mutual interaction between Hb incorporated into ZIF-67 and heteroatoms within the MOF material, with a negative effect, as in the previous analysis. Moreover, the mean binding rate of dissolved H_2O_2 with Hb attachment onto ZIF-67 can be determined to be 8.04×10^{-7} mol·s^{-1}, according to a method introduced earlier [19]. The rate constant for substrate adsorption onto the MOF material with Hb accommodation was calculated to be 2.0 s^{-1} by normalizing the previous parameter to the efficient protein surface coverage (unit: mol). Table 2 shows that, in comparison to other similar cases [45–49], the Hb-based electrode in this study displayed an undesirable affinity for the substrate. This competitive ligation is responsible for the distortion of the original configuration of the heme site in Hb. The competitive ligation between ZIF-67 and Hb contributes to the decrease in the detection limit of the negative interference in the charge transportation mechanism with increased active energy.

Figure 14d shows the dependence plot of the Levich current for the Hb-based electrode in PBS containing H_2O_2 against the square root of the electrode rotation rate. The electrode rotating velocity window maintains a good linear relationship. The deviation from the linear fit curve under higher electrode rotation rates is shown in Fig. 14d. This characteristic can be ascribed to Hb desorption from the surface of ZIF-67, resulting from the relatively weak interaction between Hb and the MOF material in the presence of a strong stress force from electrode rotation. Furthermore, the apparent diffusion rate coefficient of H_2O_2 (Da) can be extrapolated from the slope of the linear fit curve to be 2.9×10^{-5} cm^2·s^{-1}, according to the related equation

Table 2 The comparison in the sensing function to dissolved hydrogen peroxide for the as-prepared Hb-based electrode with other similar cases

Modified electrodes	Sensitivity ($A \cdot L \cdot mol^{-1}$)	Detection limit (mM)	K_M (mM)	Refs
Hb/PAn–SiO_2/DTAB/CPE	-	2.8	0.275	[45]
HbNPs/Au electrode	1.3×10^{-3}	1.0×10^{-3}	0.1	[46]
Hb/CuO/CPE	-	7.0×10^{-4}	0.03	[47]
CsNFs-SDS-Hb/AuE	-	5.0×10^{-5}	9.61×10^{-3}	[48]
Hb-Pd@Fe_3O_4-MWCNT/GCE	-	6.3×10^{-5}	0.021	[49]
Hb@ZIF-67/GCE	4.4×10^{-4}	8.9×10^{-3}	0.194	This work

mentioned elsewhere [50]. The normalized diffusion rate of the substrate can be determined to be 1.9×10^{-3} s^{-1} from the normalization of D_a to the surface active area of ZIF-67 with Hb attachment. Based on the analysis of the kinetic parameters involved in the Hb-induced electroreduction of H_2O_2, one can conclude that the efficiency of the electrocatalytic process is primarily determined by substrate mass transfer. Notably, this conclusion is based solely on objective data. The electrocatalytic performance is not significantly affected by mutual interactions between Hb and ZIF-67.

The experimental results for the reproducibility (a) and long-term usability (b) of Hb-involved electrocatalysis for H_2O_2 reduction (Hb-based electrode in PBS with dissolved H_2O_2) are shown in Fig. 15. The steady catalytic currents for the nine as-prepared Hb-based electrodes differed only slightly, as suggested by the results in Fig. 15a. The relative standard deviation (*RSD*) of the electrocatalytic current response of nine Hb@ZIF-67/GCE electrodes in the same batch was ~ 5.5%. The results reveal favorable repeatability of the catalytic effect of the as-prepared Hb-based electrode, which can be ascribed to the moderate interaction strength between Hb and ZIF-67 that retains the original configuration of heme sites within Hb to a great extent. Furthermore, the residual enzymatic activity for substrate reduction decreases as the incubation period increases. The residual activity remained at approximately 80% of the initial activity of the Hb-based electrode after storage for 9 days. This attenuation in Hb-induced electrocatalysis

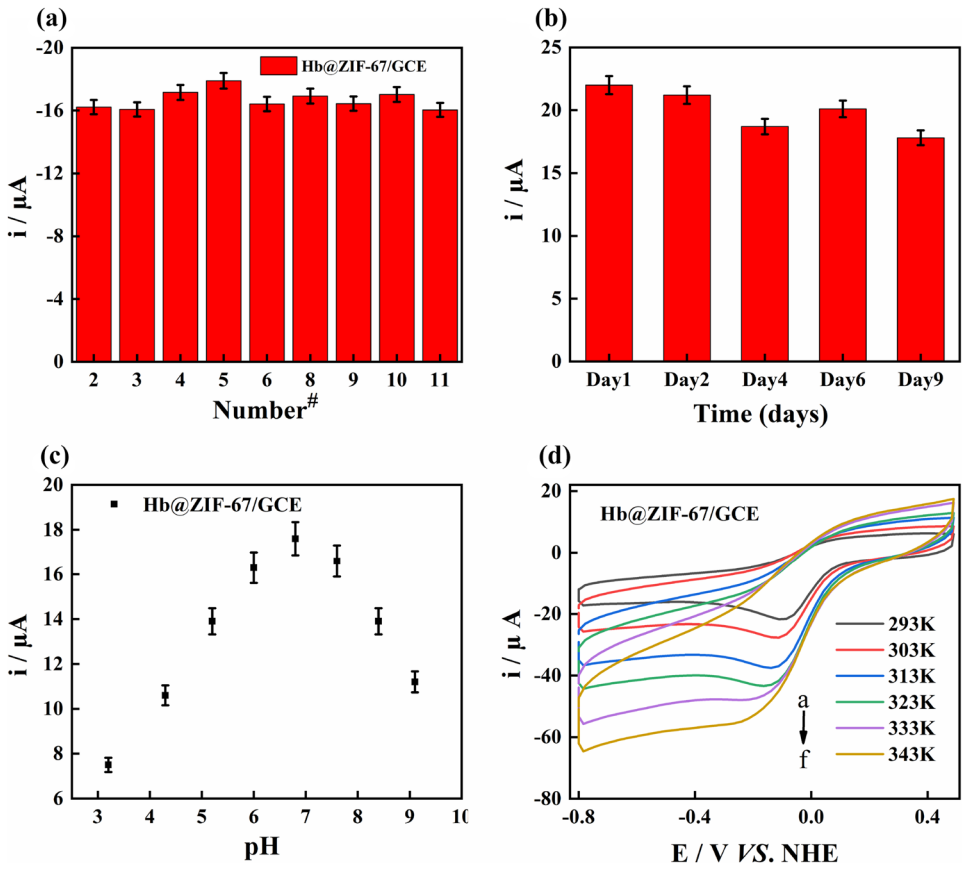

Fig. 15 The experimental results in the reproducibility (**a**), long-term usability (**b**) in Hb-involved electro-catalysis on H_2O_2 reduction (Hb-based electrode in electron relay-free and neutral PBS with 7.3×10^{-5} $mol \cdot L^{-1}$ H_2O_2); the electro-catalytic reduction current for Hb-based electrode and environmental pH (**c**); the relationship curve of the electro-catalytic effect on H_2O_2 reduction for Hb-based electrode in PBS containing hydrogen peroxide versus operational temperature (**d**)

can be attributed to the denaturation of the immobilized heme protein molecules. This assumption was confirmed by additional spectrometric tests, which indicated that the diagnostic peak at ~ 405 nm for the Soret band of native Hb was considerably diminished after Hb incubation in discrete ZIF-67 for 10 days. The amide II band in the FTIR spectrum of ZIF-67 with Hb accommodation was significantly crippled after incubation of the MOF material with Hb anchoring for 10 days (the related data are not presented).

The relationship between the steady electrocatalytic reduction current of the Hb-based electrode and the environmental pH is shown in Fig. 15c, and it is similar to that of the free native heme protein (i.e., the bell shape; data not provided here). The optimal pH value for Hb immobilization onto ZIF-67 was 6.8, indicating that the nature of the immobilized metal redox protein molecule is similar to that of native Hb from the intact configuration of the cofactor in Hb in the presence of moderate interactions between the protein and MOF. The dependence CVs of static Hb-based electrodes in neutral PBS containing 1.5×10^{-5} mol·L^{-1} H_2O_2, recorded at a potential sweeping rate of 200.0 mV·s^{-1} at operation temperatures, are shown in Fig. 15d. The steady electrocatalytic current for Hb@ZIF-67/GCE is continuously enhanced with increasing operational temperature. The onset potential of electroreduction remains stable with increasing experimental temperature. An increase in temperature leads to significant decomposition of the Hb complex with ZIF-67, which restores the inherent electrocatalytic activity of Hb to a certain extent. Furthermore, Hb desorption from the electrode surface with the ZIF-67 overcoating contributes to the attenuation of the electroreduction current. This characteristic indicates that the electrocatalytic efficiency is crippled when the temperature is higher than 348 K (data not shown). This finding demonstrates that Hb attachment onto ZIF-67 is dominated by typical chemical adsorption from the synergy of H-bond interactions and the competitive ligation of Hb with ZIF-67.

Conclusion

Cobalt nitrate hexahydrate and 2-methylimidazole were used as raw materials to prepare a typical MOF, ZIF-67, to accommodate heme protein molecules via the collaborative effect of H-bond interactions and competitive ligation. ZIF-67 acted as an enzyme carrier and protector in the inherent configuration of native Hb. The influences of the mutual interactions between the heme protein and MOF material on the electron shuttle mechanism and the electrocatalytic efficiency of H_2O_2 reduction were evaluated and analyzed. The weaker interaction between the metalloprotein and ZIF-67 did not engender a novel crystalline surface or any significant variation in the configuration of the cofactor within Hb. However, the competitive coordination between Hb and ZIF-67 resulted in a remarkable shift in the amide II band and an improvement in the surface hydrophilicity of ZIF-67 with heme protein attachment. Direct electron transfer between the heme site in Hb and the conductive surface of the enzyme support was achieved with moderate kinetics (~ 0.1 s^{-1}). The competitive complexation of Hb with ZIF-67 cannot impose a serious impact on the electron transportation route. The charge conveyance could be dominated by electrically wired Hb incorporation into ZIF with the similar feature to the free state of native heme protein. The presence of electrically wired Hb promoted the electrocatalysis on H_2O_2 reduction substantially with increasing magnitude of the electrocatalytic current response. The coalescence of Hb with ZIF-67 resulted in a relatively moderate affinity to the substrate ($K_M = 194.0$ μM) and an unfavorable detection limit (8.9 μmol·L^{-1}). The determining step in restraining the electrocatalytic performance of Hb-based electrode was the substrate mass-transfer procedure. This characteristic indicated that the mutual interactions between the heme protein and ZIF-67 did not influence the Hb-mediated electrocatalysis of H_2O_2.

Supplementary Information The online version contains supplementary material available at https://doi.org/10.1007/s10008-024-05955-x.

Author contribution Jian Ming Wang implements the additional supplements of experimental data to consolidate the conclusions in the manuscript. He also participates in the analysis to the electrochemical data and the main deduction in the submission. Xue Qing Chu provides most data of spectrometric and electrochemical experiments. She makes the relevant explanation. Han Zeng is responsible for the sections of the abstract and the conclusion. He contributes to the preparation of the whole framework in the main manuscript text and gets involved in the data analysis. All the authors commented on the previous versions of the manuscript. All the authors read and approved the final manuscript.

Funding The project was financially sponsored by the Natural Science Foundation of Xin-Jiang Uygur Autonomous Region (2022D01A209) and the "13th five-year" plan for key discipline chemistry, Xinjiang Normal University.

Data and material availability The data to support the findings of the investigation are available on request from the corresponding author, Han ZENG, upon reasonable request. Han ZENG as the corresponding author has the responsibility to the current submission.

Declarations

Conflict of interest The authors announce that no known competing financial interests or personal relationships to impose considerable impact on the work presented in this submission. No conflict of interest existed in this manuscript. This manuscript is endorsed by all anonymous authors listed in this work. All the authors of this manuscript have approved that relevant information about them is accurate and the description about their contributions is appropriate. The submission to this

journal was on the basis of original research. The content of this manuscript has not been published or described previously whether it is a whole or a part. The authors declare that they have no conflict of interest.

References

1. Chen J, Liu K, Jiang M, Han J, Liu M, Wang C, Li C (2019) Controllable preparation of porous hollow carbon sphere@ZIF-8: novel core-shell nanomaterial for Pb^{2+} adsorption. Colloids Surf A 568:461–469
2. Song JY, He WT, Shen H, Zhou ZX, Li MQ, Su P, Yang Y (2019) Construction of multiple enzyme metal-organic frameworks biocatalyst via DNA scaffold: a promising strategy for enzyme encapsulation. Chem Eng J 363:174–182
3. Cui JD, Ren SZ, Sun BT, Jia SR (2018) Optimization protocols and improved strategies for metal-organic frameworks for immobilizing enzymes: current development and future challenges. Coord Chem Rev 370:22–41
4. Wang RY, Yin YJ, Wang RQ, Xie YZ, Ge BY, Li ZG, Li Z, Shi J (2013) Study of the interaction between bovine hemoglobin and analogs of biphenyldicarboxylate by spectrofluorimetry. J Lumin 144:79–86
5. Zhang C, Wang XR, Hou M, Li XY, Wu XL, Ge J (2017) Immobilization on metal-organic framework engenders high sensitivity for enzymatic electrochemical detection. ACS Appl Mater Interfaces 9(16):13831–13836
6. Wu XL, Ge J, Yang C, Hou M, Liu Z (2015) Facile synthesis of multiple enzyme-containing metal-organic frameworks in a biomolecule-friendly environment. Chem Commun 51(69):13408–13411
7. Tan SY, Long Y, Han Q, Guan HY, Liang QL, Ding MY (2020) Designed fabrication of polymer-mediated MOF-derived magnetic hollow carbon nanocages for specific isolation of bovine hemoglobin. ACS Biomater Sci Eng 6(3):1387–1396
8. Lykourinou V, Chen Y, Wang XS, Meng L, Hoang T, Ming LJ, Musselman RL, Ma SQ (2011) Immobilization of MP-11 into a meso-porous metal-organic framework, MP-11@ meso-MOF: a new platform for enzymatic catalysis. J Am Chem Soc 133(27):10382–10385
9. Shi S, Zhang WT, Wu HF, Li YC, Ren XY, Li M, Li J, Sun J, Yue TL, Wang JL (2020) In situ cascade derivation toward a hierarchical layered double hydroxide magnetic absorbent for high-performance protein separation. ACS Sustainable Chem Eng 8(12):4966–4974
10. Filip J, Andicsova-Eckstein A, Vikartovska A, Tkac J (2017) Immobilization of bilirubin oxidase on graphene oxide flakes with different negative charge density for oxygen reduction. The effect of GO charge density on enzyme coverage, electron transfer rate and current density. Biosens Bioelectron 89:384–389
11. Traunsteiner C, Sek S, Huber V, Valero-Vidal C, Kunze-Liebhäuser J (2016) Laccase immobilized on a mixed thiol monolayer on Au (111)-structure-dependent activity towards oxygen reduction. Electrochim Acta 213:761–770
12. Szamocki R, Flexer V, Levin L, Forchiasin F, Calvo EJ (2009) Oxygen cathode based on a layer-by-layer self-assembled Laccase and osmium redox mediator. Electrochim Acta 54(7):1970–1977
13. Tian YQ, Zhao YM, Chen ZX, Zhang GN, Weng LH, Zhao DY (2007) Design and generation of extended zeolitic metal-organic frameworks (ZMOFs): synthesis and crystal structures of zinc(II) imidazolate polymers with zeolitic topologies. Chem - Eur J 13(15):4146–4154
14. Zheng JG, Lin Z, Lin G, Yang HH, Zhang L (2015) Preparation of magnetic metal-organic framework nanocomposites for highly specific separation of histidine-rich proteins. J Mater Chem B 3(10):2185–2191
15. Chu YY, Hou JW, Boyer C, Richardson JJ, Liang K, Xu JT (2018) Biomimetic synthesis of coordination network materials: recent advances in MOFs and MPNs. Appl Mater Today 10:93–105
16. Zhou YL, Li XQ, Pan ZH, Ye BX, Xu MT (2019) Determination of malachite green in fish by a modified MOF-based electrochemical sensor. Food Anal Methods 12(5):1246–1254
17. Chen YT, Wang F, Zhang M, Zeng H (2022) The catalytic effect on H_2O_2 electro-reduction of an electrode based on MOF material ZIF-8 as hemoglobin supporter via hydrogen bond interaction. J Electron Mater 51:4493–4508
18. Zhang ZJ, Zhang M, Cai YJ, Fan WG, Zeng H (2022) Investigation to the impact of mutual interactions between CdS sensitized TiO_2 and integrated Hemoglobin on the catalysis of H_2O_2 Electro-reduction. Chem Phys 562:111664
19. Li JX, Tang J, Zhou LH, Han X, Liu HL (2012) Direct electrochemistry and electrocatalysis of hemoglobin immobilized on polyacrylamide-P123 film modified glassy carbon electrode. Bioelectrochemistry 86:60–66
20. Liu XJ, Chen WW, Lian ML, Chen X, Lu YL, Yang WS (2019) Enzyme immobilization on ZIF-67/MWCNT composite engenders high sensitivity electrochemical sensing. J Electroanal Chem 833:505–511
21. Chu XQ, Zhang M, Huo WS, Zeng H, Yang Y (2020) 2-Hydroxy-4-amino-azobenzene modified graphene oxide with incorporation of Bilirubin oxidase for photoelectrochemical catalysis of oxygen reduction reaction. Int J Electrochem Sci 15:11531–11554
22. Qiu HJ, Xu CX, Huang XR, Ding Y, Qu YB, Gao PJ (2009) Immobilization of Laccase on nanoporous gold: comparative studies on the immobilization strategies and the particle size effects. J Phys Chem C 113(6):2521–2525
23. Qian JF, Sun F, Qin LZ (2012) Hydrothermal synthesis of zeolitic imidazolate framework-67 (ZIF-67) nanocrystals. Mater Lett 82:220–223
24. Sun KW, Wang F, Ma TM, Zeng H (2022) Investigation on impact of mutual interactions between elements of Ag nano-particle core-MOF material shell nano-complex and incorporated hemoglobin on electro-catalysis on H_2O_2 electro-reduction. Chem Pap 76:2703–2719
25. Xu JW, Ma TM, Zhang M, Zeng H (2021) Electro-catalysis on H_2O_2 reduction of electrode capped by nanotubes-polypyrrole composite with hemoglobin integration. J Mater Sci: Mater Electron 32:6064–6079
26. Nadar SS, Rathod VK (2019) One pot synthesis of α-amylase metal organic framework (MOF)-sponge via dip-coating technique. Int J Biol Macromol 138:1035–1043
27. Tuan DD, Andrew Lin KY (2018) Ruthenium supported on ZIF-67 as an enhanced catalyst for hydrogen generation from hydrolysis of sodium borohydride. Chem Eng J 351:48–55
28. Tang J, Yang C, Zhou L, Ma F, Liu SC, Wei SH, Zhou JH, Zhou YH (2012) Studies on the binding behavior of prodigiosin with bovine hemoglobin by multi-spectroscopic techniques. Spectrochimica Acta Part A 96:461–467
29. Charbgoo F, Nejabat M, Abnous KK, Soltani F, Taghdisi SM, Alibolandi M, Shier WT, Steele T, Ramezani M (2018) Gold nanoparticle should understand protein corona for being a clinical nanomaterial. Journal of Controlled Release Official Journal of the Controlled Release Society 272:39–53
30. Henzler K, Wittemann A, Breininger E, Ballauff M, Rosenfeldt S (2007) Adsorption of bovine hemoglobin onto spherical polyelectrolyte brushes monitored by small-angle X-ray scattering and Fourier transform infrared spectroscopy. Biomacromol 8(11):3674–3681
31. Fu XY, Li JZ, Li DD, Zhao LJ, Yuan ZY, Shulga V, Han W, Wang LL (2022) Mxene/ZIF-67/pan nanofiber film for ultra-sensitive pressure sensors. ACS Appl Mater Interfaces 10:14
32. Liu XP, Wang BH, Cheng J, Meng QM, Song YX, Li MH (2020) Investigation on the capture performance and influencing factors of ZIF-67 for hydrogen sulfide. Sep Purif Technol 250:117300

33. Shi JF, Wang XL, Zhang SH, Tang L, Jiang ZY (2016) Enzyme-conjugated ZIF-8 particles as efficient and stable Pickering interfacial biocatalysts for biphasic biocatalysis. J Mater Chem B 4(15):2654–2661
34. Nadar SS, Rathod VK (2018) Encapsulation of lipase within metal-organic framework (MOF) with enhanced activity intensified under ultrasound. Enzyme Microb Technol 108:11–20
35. Qin PF, Liu RT, Teng Y (2011) Perfluorodecanoic acid binding to hemoproteins: new insights from spectroscopic studies. J Agric Food Chem 59(7):3246–3252
36. Mandal P, Ganguly T (2009) Fluorescence spectroscopic characterization of the interaction of human adult hemoglobin and two isatins, 1-methylisatin and 1-phenylisatin: a comparative study. J Phys Chem B 113(45):14904–14913
37. Zhang SW, Zhang M, Wang F, Zeng H (2022) Direct electrochemistry and enzyme-involved photo-electrocatalysis of oxygen reduction for the electrode on the basis of titanium dioxide-graphene oxide nano-complex with laccase accommodation. Chem Eng J 430:132619
38. Han R, Liu BS, Li GX, Zhang QJ (2016) Investigation on the interaction between lysozyme and cefepime hydrochloride by synchronous fluorescence and fluorescence quenching spectroscopy. Spectrosc Lett 49(3):225–230
39. Xian YZ, Xian Y, Zhou LH, Wu FH, Ling Y, Jin LT (2007) Encapsulation hemoglobin in ordered mesoporous silicas: influence factors for immobilization and bioelectrochemistry. Electrochem Commun 9:142–148
40. Zhao HY, Zhou HM, Zhang JX, Zheng W, Zheng YF (2009) Carbon nanotube-hydroxyapatite nanocomposite: a novel platform for glucose/O_2 biofuel cell. Biosens Bioelectron 25:463–468
41. Shleev S, Christenson A, Serezhenkov V, Burbaev D, Yaropolov A, Gorton L, Ruzgas T (2005) Electrochemical redox transformations of T1 and T2 copper sites in native Trametes hirsuta laccase at gold electrode. Biochem J 385:745–754
42. Farneth WE, Diner BA, Gierke TD, D'Amore MB (2005) Current densities from electrocatalytic oxygen reduction in laccase/ABTS solutions. J Electroanal Chem 581:190–196
43. Zhang Y, Zeng GM, Tang L, Huang DL, Jiang XY, Chen YN (2007) A hydroquinone biosensor using modified core-shell magnetic nanoparticles supported on carbon paste electrode. Biosens Bioelectron 22:2121–2126
44. Kong YT, Boopathi M, Shim YB (2004) Direct electrochemistry of horseradish peroxidase bonded on a conducting polymer modified glassy carbon electrode. Biosens Bioelectron 19(3):227–232
45. Chen B, Wang H, Zhang HY, He ZX, Zhang SJ, Liu T, Zhou YZ (2012) A novel hydrogen peroxide sensor based on hemoglobin immobilized PAn–SiO_2/DTAB composite film. J Mol Liq 171:23–28
46. Narwal V, Yadav N, Thakur M, Pundir CS (2017) An amperometric H_2O_2 biosensor based on hemoglobin nanoparticles immobilized onto a gold electrode. Biosci Rep 37(4):BSR20170194
47. Abbasi A, Shamsazar A, Shamsazar F, Asadi A, Shamsaldini S (2018) Hydrogen peroxide biosensor based on carbon paste modified electrode with hemoglobin and copper(II) oxide nanoparticles. Int J Electrochem Sci 13:3986–3996
48. Kholosi F, Afkhami A, Hashemi P, Madrakian T, Bagheri H (2020) Bioelectrocatalysis and direct determination of H_2O_2 using the high-performance platform: chitosan nanofibers modified with SDS and hemoglobin. J Iran Chem Soc 17:1401–1409
49. Baghayeri M, Veisi H (2015) Fabrication of a facile electrochemical biosensor for hydrogen peroxide using efficient catalysis of hemoglobin on the porous Pd@Fe3O4-MWCNT nanocomposite. Biosens Bioelectron 74:190–198
50. Tsujimura S, Kamitaka Y, Kano K (2007) Diffusion-controlled oxygen reduction on multi-copper oxidase-adsorbed carbon aerogel electrodes without mediator. Fuel Cells 7(6):463–469